

Article

Comparison of the Blade Element Momentum Theory with Computational Fluid Dynamics for Wind Turbine Simulations in Turbulent Inflow

Sebastian Ehrich ^{1,*}, Carl Michael Schwarz ¹, Hamid Rahimi ^{1,2}, Bernhard Stoevesandt ²
and Joachim Peinke ^{1,2}

¹ ForWind, University of Oldenburg, Institute of Physics, K pkersweg 70, 26129 Oldenburg, Germany; carl.michael.schwarz@uni-oldenburg.de (C.M.S.); hamid.rahimi@uni-oldenburg.de (H.R.); joachim.peinke@uni-oldenburg.de (J.P.)

² Fraunhofer IWES, K pkersweg 70, 26129 Oldenburg, Germany; bernhard.stoevesandt@iwes.fraunhofer.de

* Correspondence: sebastian.ehrich@uni-oldenburg.de; Tel.: +49-441-798-5057

Received: 30 September 2018; Accepted: 2 December 2018; Published: 6 December 2018



Abstract: In this work three different numerical methods are used to simulate a multi-megawatt class class wind turbine under turbulent inflow conditions. These methods are a blade resolved Computational Fluid Dynamics (CFD) simulation, an actuator line based CFD simulation and a Blade Element Momentum (BEM) approach with wind fields extracted from an empty CFD domain. For all three methods sectional and integral forces are investigated in terms of mean, standard deviation, power spectral density and fatigue loads. It is shown that the average axial and tangential forces are very similar in the mid span, but differ a lot near the root and tip, which is connected with smaller values for thrust and torque. The standard deviations in the sectional forces due to the turbulent wind fields are much higher almost everywhere for BEM than for the other two methods which leads to higher standard deviations in integral forces. The difference in the power spectral densities of sectional forces of all three methods depends highly on the radial position. However, the integral densities are in good agreement in the low frequency range for all methods. It is shown that the differences in the standard deviation between BEM and the CFD methods mainly stem from this part of the spectrum. Strong deviations are observed from 1.5 Hz onward. The fatigue loads of torque for the CFD based methods differ by only 0.4%, but BEM leads to a difference of up to 16%. For the thrust the BEM simulation results deviate by even 29% and the actuator line by 7% from the blade resolved case. An indication for a linear relation between standard deviation and fatigue loads for sectional as well as integral quantities is found.

Keywords: wind turbine; aerodynamics; turbulent inflow; Computational Fluid Dynamics; blade element momentum theory; actuator line method; Fatigue Loads

1. Introduction

One of the most common tools for wind turbine design and load calculation is the Blade Element Momentum method (BEM). Although BEM based tools are known to be very efficient, they are based on many simplifications. Among others, some worth mentioning are stationary environment, 2D airfoil characteristics and inviscid fluid behavior [1]. While preserving its efficiency, over the years a lot of correction models have been developed to improve the accuracy, e.g., by using tip loss or dynamic stall models. A comprehensive overview of those models can be found in the work of Schepers [1]. However, especially for turbulent inflow scenarios, the reliability of such estimations is still unknown. This is mainly due to the relatively coarse discretization of wind fields and rotor blades, the incorrect dynamic aerodynamic response to complex inflow, the unresolved flow field but also the assumption

of inviscid and stationary flow. Nevertheless, wind turbines are operating under atmospheric wind conditions and the dynamics of the forces that are acting on the blades are still unknown. Most of the effects were measured in the wind tunnel with uniform or very simplified changing inflow conditions. However, turbulent inflow scenarios are relevant to the design and certification process, e.g., to the design load cases 1.1–1.3 of the IEC standard [2]. The research conducted in this field is limited with recent studies done by Madsen et al. [3] and in the AVATAR project [4]. In both cases BEM is compared to higher fidelity codes. In the work by Madsen et al. a 2.5MW turbine was simulated with BEM and Blade Resolved (BR) Computational Fluid Dynamics (CFD) with a turbulent inflow based on the model by Mann [5]. The wind fields for BEM were extracted at the rotor position in the empty CFD domain. Additionally, measurement data of this turbine and BEM results for the same data were compared. In both cases spectra of sectional forces were investigated. In the AVATAR project similar quantities were in the focus of the study, but one Mann box was generated and used for the CFD as well as the BEM simulation. In CFD the natural decaying process of the wind fields leads to a decreased turbulence intensity and different turbulent structures at the turbine compared to BEM. Therefore the simulation results of BEM and CFD are not comparable. Also global quantities like thrust and torque as well as their corresponding fatigue loads were not investigated. Although those works are giving a valuable insight to BEM modeling uncertainties when combined with turbulent inflow, there is still a lack of comparable studies and a best practice guide for the comparison of CFD and BEM simulations is still missing.

The present work aims to compare BEM based simulations for turbulent inflow conditions with two higher fidelity CFD methods, namely the BR simulation and the Actuator Line (AL) model [6]. New in this work is the combination of the investigation of frequency resolved integral forces, the analysis of fatigue loads and a bridge between BR and BEM calculations, namely the AL method. The goal of this study is to shed light into the difficulties and expectations of the different methods proposed and information for future comparisons of CFD and BEM based simulations shall be provided.

This paper is organized as following. The basic setup of the turbine, the turbulent wind fields, the CFD and BEM simulations, and the fatigue load estimation are addressed in Section 2. In Section 3 key aerodynamic quantities of the turbine such as power, thrust and sectional forces and the corresponding equivalent fatigue loads as well as spectral properties are investigated. Finally a conclusion including future work is presented in Section 4.

2. Methodology

In this section the basic methodology used in this work concerning the wind turbine, the wind fields and the numerical setup as well as a short introduction to the fatigue load estimation procedure is presented.

2.1. The Wind Turbine Model

The numerical studies are performed on the NREL-5MW reference wind turbine with a rotor diameter of 126 m [7]. This three bladed horizontal axis wind turbine with a blade length of 61.5 m was designed by the National Renewable Energy Laboratory. It is close to the current average rotor size of newly installed wind turbines which accounts to 100–120 m. More details on the reference turbine can be found in Table 1.

Table 1. Overview of NREL-5MW turbine specification.

Parameter	Value
Number of rotor blades	3
Rotor diameter	126 m
Rated aerodynamic power	5.3 MW
Rated wind speed	11.4 m/s

Table 1. Cont.

Parameter	Value
Rated rotational speed	12.1 rpm
Blade cone angle	2.5°
Shaft tilt angle	5.0°
Blade length	61.5 m
Blade mass	17,740 kg

2.2. The Wind Fields

It is assumed that the specific inflow turbulence model does not change the general trend of the outcome of the study presented in this paper as long as some main properties of the wind fields are fulfilled like spatial and temporal correlations, Gaussianity and stationarity. However, the model used here should also be as simple as possible with a very low memory consumption which is for spectral methods usually very high if the time and space domains are large. Therefore velocity fluctuations are represented by a Gaussian process realized at the inflow patch of the CFD domain. In particular, coupled stochastic Ornstein-Uhlenbeck processes of the form

$$\frac{du_i^{(k)}(t)}{dt} = -\gamma \left(u_i^{(k)}(t) - \bar{u}^{(k)} \right) + \sqrt{D} \sum_j^N H_{ij} \Gamma_j^{(k)}(t) \quad (1)$$

with an exponentially decaying spatial and temporal correlation function for all wind components are used without taking shear into account. In this stochastic differential equation each subscript $i, j = 1 \dots N$ denotes a specific cell on the inlet patch where the turbulence is generated and each superscript $k = x, y, z$ corresponds to the longitudinal, lateral or vertical velocity component. $\gamma = 0.97 \text{ s}^{-1}$ is a damping factor, $\bar{u}^{(y,z)} = 0 \text{ ms}^{-1}$ and $\bar{u}^{(x)}$ the mean velocities in x, y and z direction, $D = 0.62 \text{ m}^2\text{s}^{-3}$ a diffusion constant, H the lower Cholesky-decomposed correlation matrix and Γ a Gaussian, delta-correlated random noise vector with variance 2.

Fields with a mean wind speed of $\bar{u}^{(x)} = 11.4 \text{ ms}^{-1}$ corresponding to the rated operating condition of the wind turbine and a Turbulence Intensity (TI) of 20% are fed into the CFD domain. This relatively high TI had to be chosen, because of the natural decaying process leading to much smaller turbulence intensities, namely 11%, in the vicinity of the turbine in the absence of shear. To make the comparison between different codes in a similar manner, the pitch and rotor speed are fixed and the effect of structural deformations, tilt and cone as well as the tower and nacelle are neglected.

2.3. Numerical Methods

In the following the BR, AL and BEM method are described in more detail:

- BR: The blade resolved simulations are performed with the CFD software OpenFOAM V4.1 [8], which is an open-source package with a collection of modifiable libraries written in C++. The simulation domain is discretized using the bladedblockMesher [9] and windTurbine mesher tools [10] with a combination of structured and unstructured grids consisting of a total of 36M cells. To exclude influences of the mesh on the solution, a mesh study has been done in our previous work [11]. The grid of the complete simulation domain and the rotating part are shown in Figure 1 and a sectional view on the mesh near the blade in Figure 2. The cell length at the inlet, which is three rotor diameters upstream of the rotor, is 1m. This mesh is uniformly extruded up to the near blade mesh where a refinement takes place and the smallest cell length of approximately 0.2 m is reached. In order to limit the cell aspect ratio in radial direction, adaptive wall functions are being applied. The solution for the flow field is achieved by solving the incompressible Delayed Detached Eddy Simulations equations. It is assumed that the flow

is fully turbulent, i.e., the laminar-turbulent transition in the boundary layer is not considered, because the inflow itself is turbulent and therefore the laminar boundary layer is not expected to have a strong influence on the blade. The closure problem is treated by use of the turbulence model proposed by Spalart et al. [12] with the proposed standard parameters. In order to solve the pressure-velocity coupling, the PIMPLE algorithm, is used, which is a combination of the loop structures of SIMPLE [13] and PISO [14]. Integration in time was performed using the implicit second order backward scheme together with the second order linear upwind scheme for discretizing the convection terms. For these simulations 360 cores were used for approximately 20 days resulting in 600 s simulation time with a time step of 0.01 s. This corresponds to 121 revolutions of the rotor.

- AL: The rotor is simplified by an AL model [6], where all rotor blades are reduced to rotating lines with a radial distribution of body forces at 60 positions along the lines. A Gaussian filtering kernel with the dimensionless smoothing parameter ε equal to 4 was used to obtain well fitting sectional forces and power output to the BR case. Based on the angle of attack at the given positions on the line, body forces are gained from lookup tables containing polars of two dimensional airfoils. A Prandtl tip [15] and root loss correction, as well as a 3D correction proposed by Du and Selig [16] are applied to the airfoil data. Except for a coarser resolution in the vicinity of the rotor with an average cell length of 1m the domain is exactly the same as for the BR case leading to a domain size of 22M cells. The flow field is simulated by Large Eddy Simulations (LES) with a Smagorinsky subgrid-scale model [17]. These simulations have been conducted on 360 cores for 25 h real time reaching 600 s simulation time with a time step of 0.01 s.
- BEM: This method uses wind fields recorded in the CFD domain on an equidistant 31×31 grid with a grid cell size of 4.5 m in both directions. In this case the fields are obtained at the position of the rotor from the same mesh as for the AL method but in an empty CFD domain. This seems to be a reasonable choice, because under this condition the TI at the rotor will be comparable for the CFD and BEM simulations. The BEM based tool FAST v8 [18] in combination with AeroDyn v15 [19] with the Beddoes Leishman type unsteady aerodynamics model [19,20] and an equilibrium wake model is used in this work. The BEM model relies on the very same airfoil data and correction models as the AL, but with only 17 blade sections. Because of the simplicity of the BEM approach the simulation with the same time stepping and total time as for the higher fidelity approaches only took two minutes on one core.

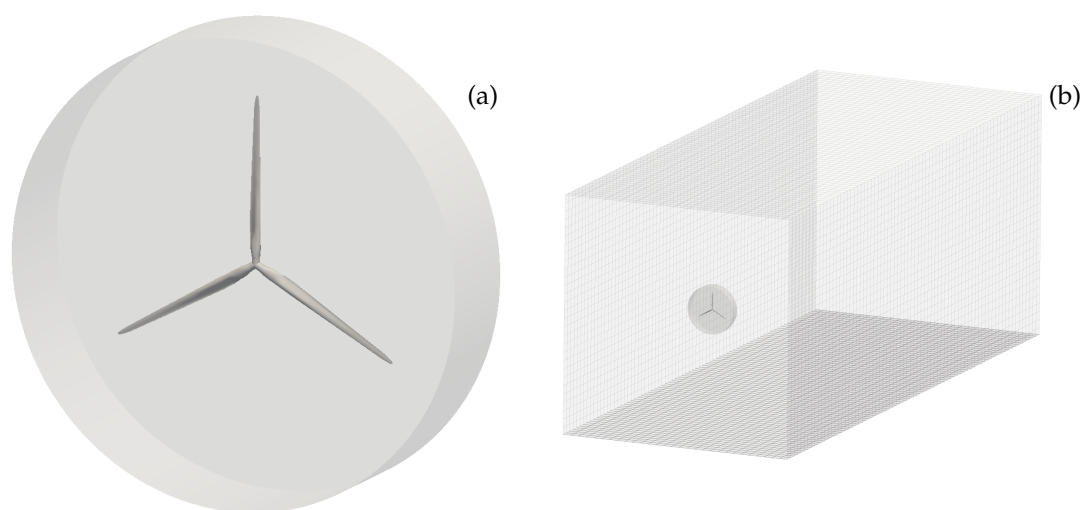


Figure 1. Grids of (a) rotating part and (b) full domain of Blade Resolved (BR) simulation.

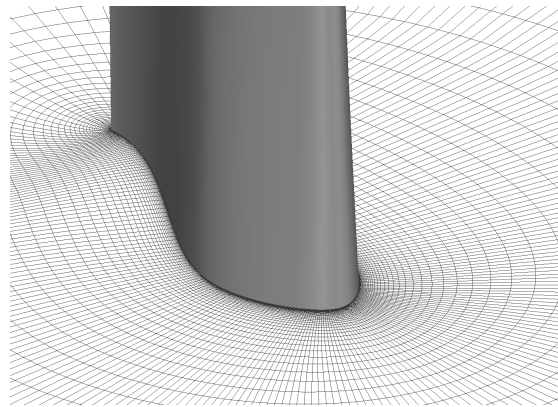


Figure 2. View onto the grid at the pressure side of the rotor blade.

2.4. Fatigue Load Estimation

One of the most important quantities relevant for wind turbine designs are the fatigue loads on different parts of the turbine estimated by damage equivalent loads. They are also known as Equivalent Fatigue Loads (EFL), which will play a role in the load analysis of the three methods investigated here. EFL can be defined as

$$EFL = \left(\frac{\sum n_i r_i^m}{T} \right)^{\frac{1}{m}}, \quad (2)$$

where r_i are the specific load ranges, n_i the corresponding amount of load ranges, T the reference number of ranges (here the dimensionless time in seconds) and $m = 8$ the Wöhler exponent. More information on the estimation of the EFL and the underlying rainflow algorithm can be found in [21,22].

3. Results

In this section the results of this study are presented. The focus lies on the wake structure, average and standard deviation of sectional and integral forces, as well as fatigue loads and Power Spectral Densities (PSD).

3.1. Wake Dynamics

Snapshots of the velocity magnitude for the BR and AL cases are shown in Figure 3. Despite the differences in the methods both simulations show similar fields in terms of the velocity magnitude upstream of the turbine. This leads to the conclusion that the induction zone of the turbine is also similar for both simulations. For a more detailed view of the similarities and differences of the two compared CFD methods the wake structure is analyzed by the time series of the main stream component at 0.5, 1 and 2 diameters at the centerline downstream of the nacelle in Figure 4. It can be seen that the wind velocity is in good agreement in most time intervals. As a quantitative measure of similarity of the wake structure, the coefficients for the correlation between both simulations are calculated by

$$\rho(x) = \frac{\langle (u_{AL}(x,t) - \bar{u}_{AL}(x)) (u_{BR}(x,t) - \bar{u}_{BR}(x)) \rangle_t}{\sigma_{AL}(x) \sigma_{BR}(x)} \quad (3)$$

where we used the time averaging operation $\langle \cdot \rangle_t$, the standard deviations σ_{AL} and σ_{BR} and the local mean values \bar{u}_{AL} and \bar{u}_{BR} of the time series of AL and BR simulations. The correlation is 0.54, 0.41 and 0.51 for 0.5, 1 and 2 diameters downstream, respectively. This shows that the wind field dynamics are rather similar and not uncorrelated at different distance from the rotor for both simulation methods. However, the BR simulation is resolving the tip and root vortex in a more physical way which results in smaller structures in the near wake.

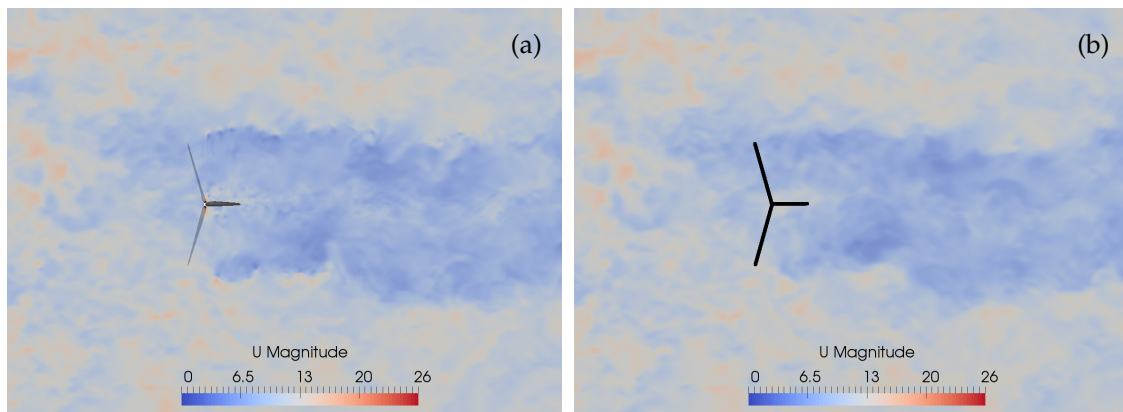


Figure 3. Snapshots of the velocity magnitude for (a) BR and (b) Actuator Line (AL) simulations.

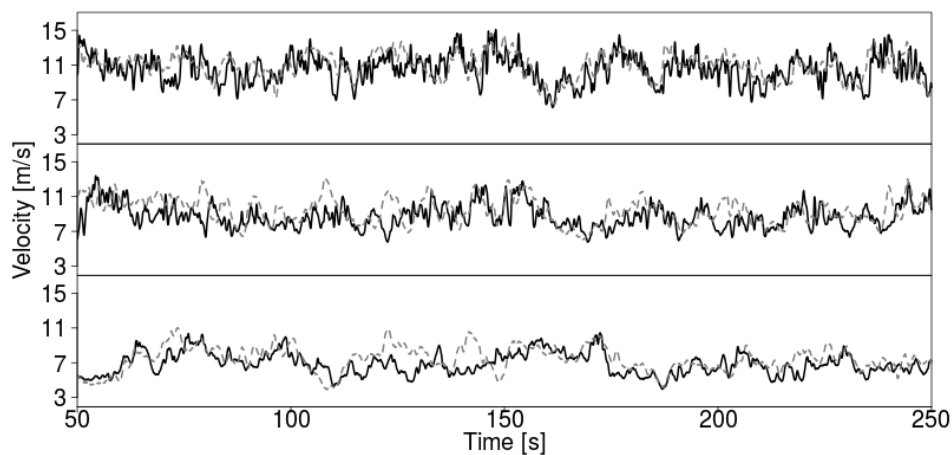


Figure 4. Wind velocity time series of BR (black, solid) and AL (grey, dashed) simulation for 0.5, 1 and 2 diameters (from top to bottom) at the centerline downstream of the rotor nacelle.

3.2. Sectional Forces

All three simulation methods (BR, AL and BEM) are compared based on averaged sectional quantities, namely axial and tangential forces, the corresponding standard deviations and the EFLs. The sectional axial and tangential forces on the blade do not reveal big differences for the average between all cases in the mid-span as shown in Figure 5. However at the root (up to 30% of span) and the very tip (from 80% of span onwards) some differences can be observed. BEM and AL rely on similar root and tip correction models and the very same airfoil data which explains their good agreement. In comparison to the more realistic BR case, where 3D effects are modeled physically, the forces at the root and tip section are far off supporting the well known issues with 3D effects for BEM and AL. The more developed vortices in the BR simulation induce much higher loads in the root and tip region than for the other methods.

The standard deviations for the tangential and axial force distributions, shown in more detail in Figure 6, are very different for all three methods. With the BR case as the reference the standard deviation of sectional forces tend to be lower at the root of the blade for the BEM and AL methods whereas they are larger in the mid-span. Close to the tip at approximately 95% of the blade the AL method gives much smaller values while BEM is in the range of the BR simulation. The corresponding errors are estimated by following three steps. In the first step the time series for the specific forces at each radial position are separated into five distinct sub time series. In the second step the standard

deviation for each sub time series is calculated. Finally the standard deviation of the set of the standard deviations from the second step is computed which provides the error for the whole time series.

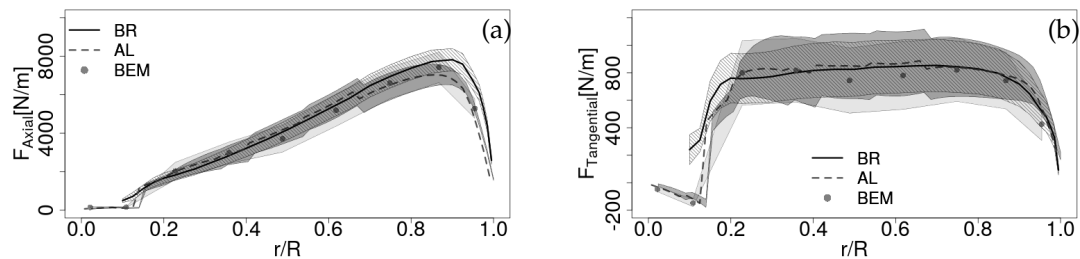


Figure 5. Radial distributions of (a) axial and (b) tangential forces per unit span. The shaded areas illustrate one standard deviation of the fluctuations.

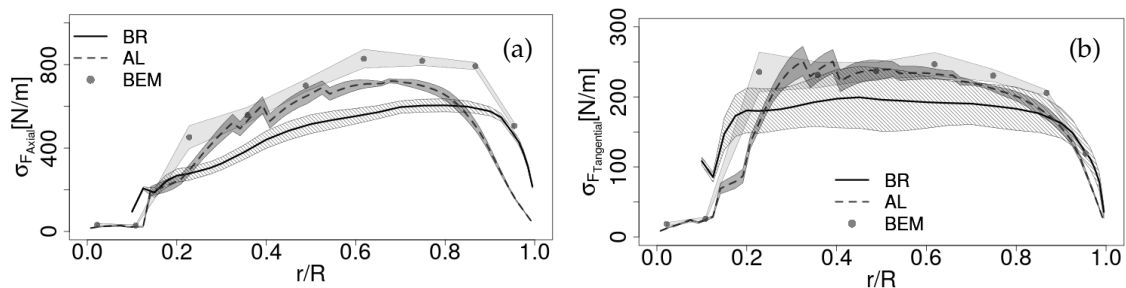


Figure 6. Radial distribution of standard deviation of (a) axial and (b) tangential forces per unit span. The shaded areas correspond to errors.

A more detailed insight in the standard deviation is gained by looking at the PSDs of axial and tangential forces at 22%, 50%, 75% and 95% radial position, shown in Figures 7 and 8.

All blade sections have in common that the spectra of the highly resolved BR case drop fastest between 2 and 10 Hz to a constant noise level. This is due to the expected bigger structures generated by the blade geometry but also due to the DDES model which is treated as RANS in the boundary layer acting as a filter.

For the AL method the energy drop happens at much higher frequencies because of the missing geometry and the LES model, which generally filters at smaller scales. The noisy behavior at high frequencies is part of every simulation of this kind and is due to numerical instabilities resulting from the convolution of the forces given at the airfoil sections with a Gaussian kernel [23].

The BEM spectra show filtering effects at higher frequencies corresponding to a multiplication with a *sinc*-like-function but with different frequencies for different radial positions. The origin of this effect could not be found and has to be investigated further. Due to the missing geometry and the lack of unsteady wake effects BEM is also expected to make worse predictions than the higher fidelity methods in the high frequency range. Therefore this high frequency part has to be taken with care like for the other two methods with their aforementioned problems of smoothing for the AL and the RANS treatment for the BR case and none of them can be considered trustworthy in this range.

In the low frequency range, for axial as well as tangential forces it can be observed that in comparison to the other two methods BEM has a much higher energy content for the inboard section. This is responsible for the high standard deviation at this section.

At radial position of 50% and 75% of the blades all the spectra are very similar in the low frequency range but it is still obvious that BEM has a higher energy content up to the 1P frequency, especially for the axial forces. Furthermore all three methods are able to capture the 1P frequency which is based on the passing of the blades through long time correlated structures.

At the outboard section at 95% the energy content of the BEM results in low frequencies is in the same range as for the BR case, but the AL method shows significant smaller values and the 1P frequency is not captured anymore, especially for the axial forces, which is due to a smeared out tip vortex.

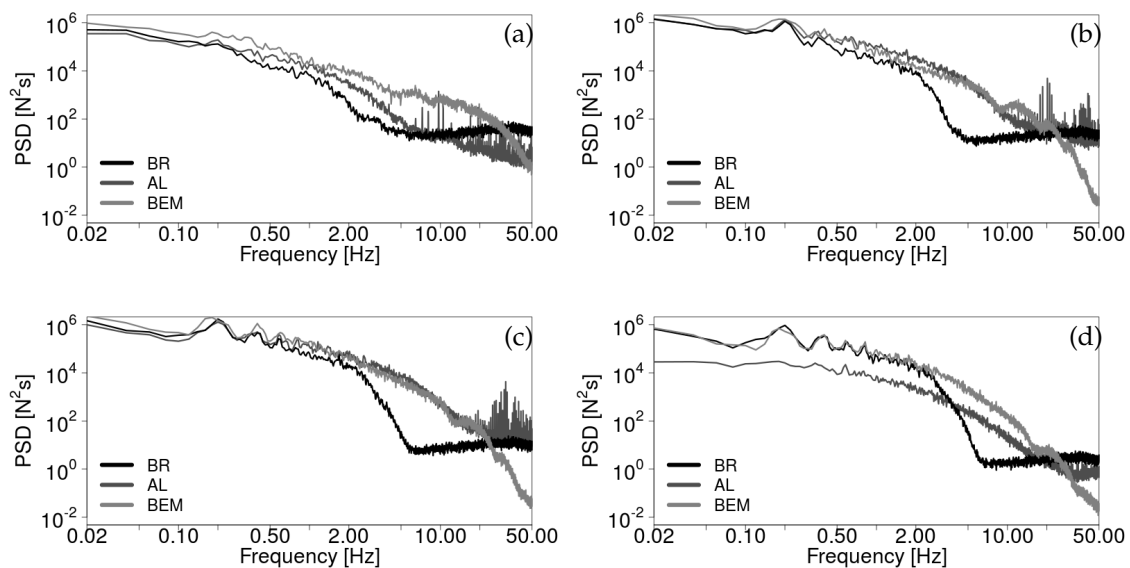


Figure 7. Power Spectral Density (PSD) of axial forces at (a) 22.5%; (b) 50%; (c) 75% and (d) 95% radial position.

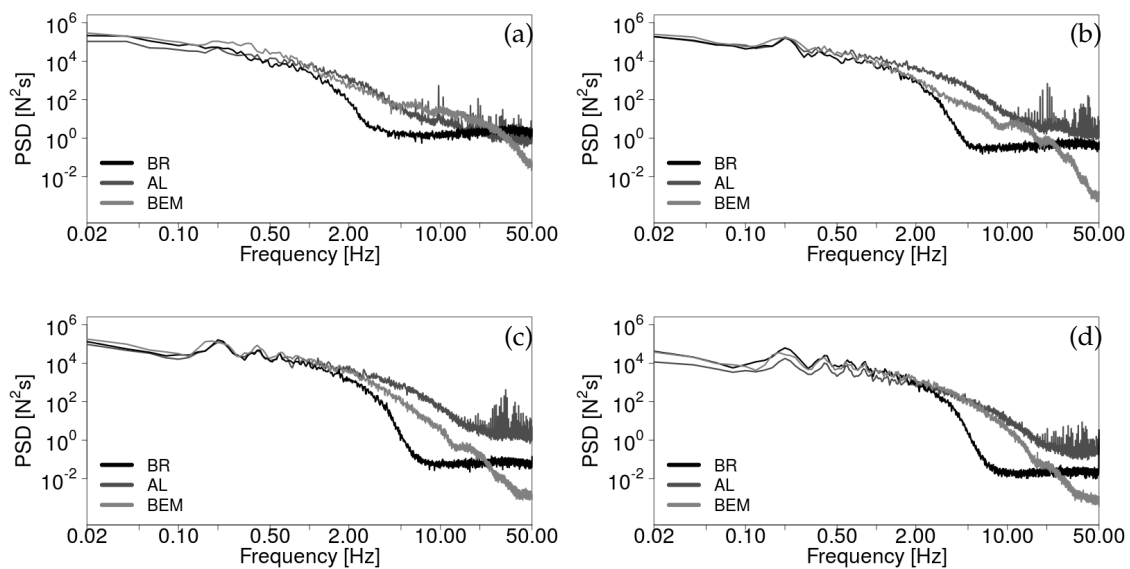


Figure 8. PSD of tangential forces at (a) 22.5%; (b) 50%; (c) 75% and (d) 95% radial position.

To illustrate the different flow structure sizes in the different simulation methods, the two point correlation of the sectional forces along the blade are measured. The argument for this approach is that the correlation of sectional forces is similar to the correlation of the wind velocity close to the blade surface, which is strongly connected to the integral scales of wind. In Figure 9 the correlation at each radial position with the forces at a reference position, here 22.5% radial location, is shown. This specific position is in principle arbitrary, but if the focus lies on the measurement of big structures, this point should not be too close to the tip or root where smaller flow structures dominate. However,

even if the tendency for the correlation functions of the three different models is the same, the larger correlation values for the BR case along the whole blade indicate that the structure sizes are also bigger than for the AL and BEM cases.

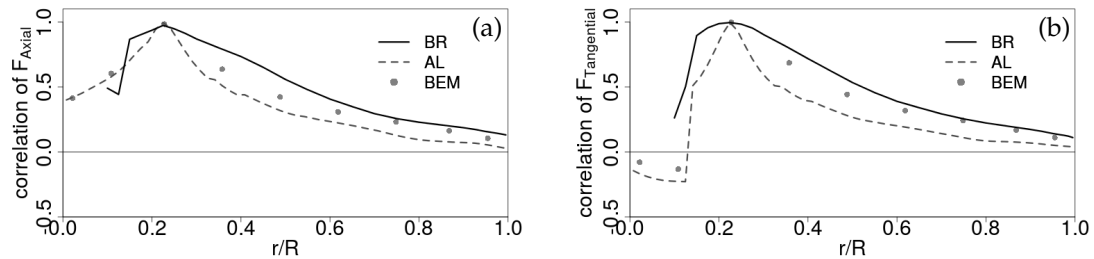


Figure 9. Correlation of (a) axial and (b) tangential forces at different radial positions with 22.5% position.

To give a more detailed description of the effect of forces on the rotor blades, fatigue loads at each section have been investigated. As observed in Figure 10, the EFL distribution over the whole blade is similar to the distribution of standard deviation in Figure 6. The BEM method gives higher EFL for every section for axial forces and almost everywhere higher values for tangential forces. All other points mentioned for sectional standard deviations also hold for sectional EFL. The errors are calculated with the same method as for Figure 6.

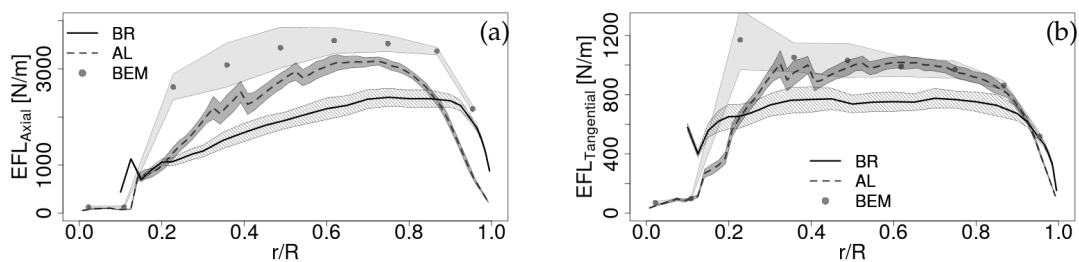


Figure 10. Radial distribution of (a) axial and (b) tangential equivalent fatigue loads per unit span. The shaded areas correspond to the errors.

The sectional EFL are linearly dependent on the sectional standard deviation for all simulation methods as seen in Figure 11. This raises the point that the dynamics quantified by two different properties of the load time series, namely standard deviation and EFL, are similar for all three methods. With the Wöhler Exponent $m = 8$ and the wind fields used here, this linear relation follows approximately $EFL = 4\sigma$ for axial and tangential forces.

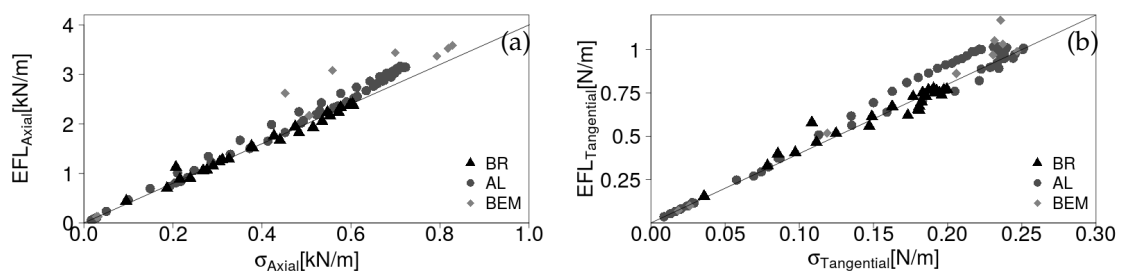


Figure 11. Equivalent Fatigue Loads (EFL) dependence on standard deviation for (a) axial and (b) tangential forces for all three methods. The diagonal line is governed by $EFL = 4\sigma$.

3.3. Integral Forces

In the following, integral forces resulting from sectional forces from Section 3.2 are discussed. Time series of the aerodynamic thrust and torque are shown in Figure 12. As can be observed, the thrust as well as the torque evolution is very similar for BR and AL. With the definition of the correlation coefficient

$$\rho = \frac{\langle (F_1(t) - \bar{F}_1) (F_2(t) - \bar{F}_2) \rangle_t}{\sigma_1 \sigma_2} \quad (4)$$

where F_1 and F_2 are the considered forces and σ_1 and σ_2 the corresponding standard deviations, the correlation is calculated as 0.90 and 0.93 for thrust and torque respectively, even if the distribution of sectional forces and the wake dynamics are more different (see Figures 4–6). A comparison between BR and BEM reveals a much smaller correlation with values of 0.08 and 0.09 for thrust and torque. This supports the argument that the wind dynamics are handled in a very different way for BEM and CFD simulations for the current setup.

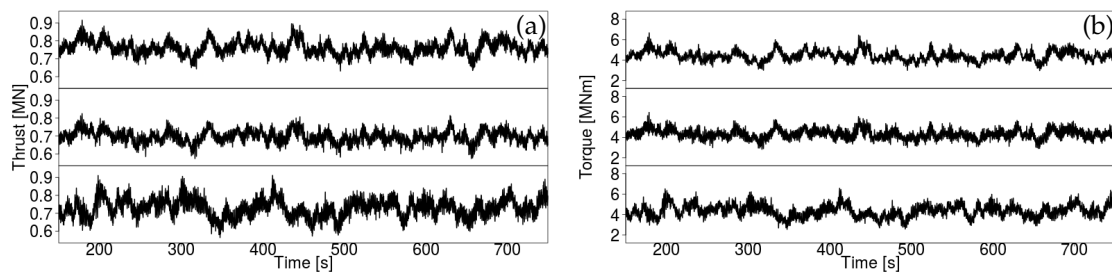


Figure 12. Time series for (a) thrust and (b) torque for Blade Resolved (BR), Actuator Line (AL) and Blade Element Momentum (BEM) methods (from top to bottom).

In Table 2 the means, standard deviations and EFLs of torque and thrust for all three methods are illustrated with their corresponding errors. Those errors are obtained by separating the corresponding time series' into five distinct equally sized ensembles and calculating the ensemble standard deviation. For comparison reasons the ratios of the calculated quantities for AL and BR as well as BEM and BR are shown, because the BR case is assumed to be the highest fidelity approach. For aerodynamic thrust and torque AL and BEM show lower values than the BR case with a minimum ratio of 91.7%, which can also be estimated from the sectional forces in Figure 5.

Table 2. Thrust and torque comparison by mean, standard deviation σ and EFL between BR, AL and BEM.

		BR	AL	BEM	AL/BR [%]	BEM/BR [%]
Thrust [kN]	mean	761 ± 7.3	698 ± 4.0	729 ± 9.6	91.7	95.8
	σ	37.9 ± 4.3	33.9 ± 2.6	49.7 ± 6.5	89.4	131.1
	EFL	147.6 ± 9.7	136.7 ± 4.2	190.1 ± 8.0	92.6	128.8
Torque [MNm]	mean	4.43 ± 0.10	4.32 ± 0.08	4.35 ± 0.13	97.5	98.2
	σ	0.495 ± 0.044	0.452 ± 0.038	0.599 ± 0.061	91.3	121.0
	EFL	1.90 ± 0.15	1.90 ± 0.13	2.29 ± 0.12	99.6	116.0

Analog to the relation between mean sectional forces and mean integral forces, the standard deviations of tangential and axial forces in Figure 6 correspond to a standard deviation in the thrust and torque. The standard deviation for the AL case is for both quantities approximately 10% smaller than for the BR simulation, because of the missing variance in the root and tip region. Especially for the torque the tip region plays a significant role. In contrast to that, for the BEM simulation an approximately 20 to 30% increase in the standard deviation is obtained which is also very clear from the much higher sectional standard deviation except at the root. A reason for the high standard

deviation could be the equilibrium wake model used here, where the wake dynamics are not captured in a proper way. The relation between EFL and the standard deviation of integral forces is shown in Figure 13 where we additionally added the diagonal line governed by $EFL = 4\sigma$ like for sectional forces in Figure 11. Sectional as well as integral forces seem to follow the same linear trend.

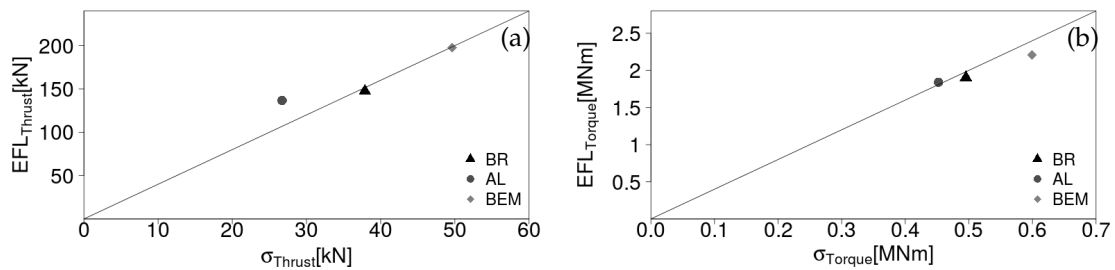


Figure 13. EFL dependence on standard deviation for (a) thrust and (b) torque for all three methods. The diagonal line is governed by $EFL = 4\sigma$.

Further analysis of the EFL by the underlying range histograms in Figure 14 shows that for the thrust and torque all three methods have in general a similar trend. But especially in the moderate ranges for the thrust and for large ranges in both quantities BEM has more counts than AL and BR. Due to their large weight the most important part for the EFLs are the high ranges. Those high ranges must not be neglected, even if they have very few counts, because very important quantities like the difference of global maxima and minima and the standard deviation contribute to them. Also the similarity of the inflow conditions justifies the comparison of the loads. The contribution of all ranges to the EFLs in Equation (2), namely $n \cdot r^m$, is shown in Figure 15, where the big contribution of the highest ranges to fatigue loads is very clear.

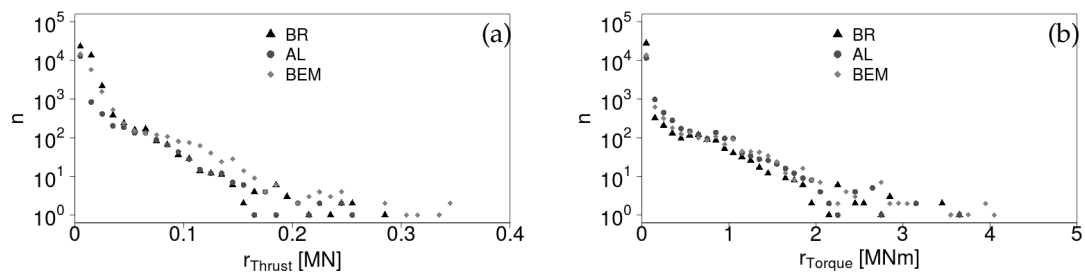


Figure 14. Range histograms for (a) thrust and (b) torque.

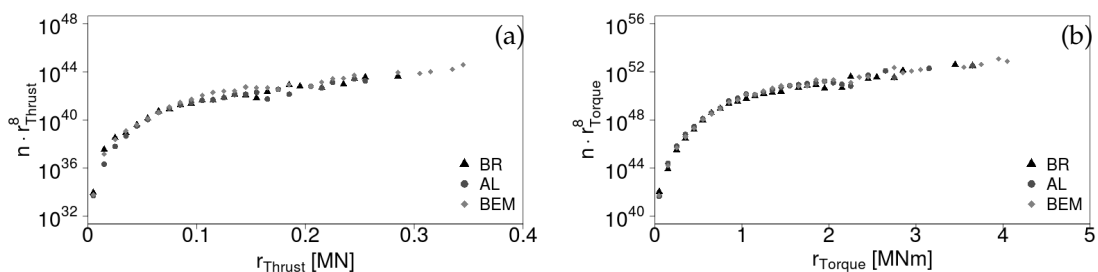


Figure 15. Contribution of ranges to EFL for (a) thrust and (b) torque.

For an analysis of the dynamics of torque and thrust, PSDs are investigated and shown in Figure 16. All three methods show a very good agreement in the shape of spectra for low frequencies in region I up to 1.5 Hz including the 3P frequency and the first harmonic. For higher frequencies up

to approximately 4 Hz, here region II, BEM and AL are very similar but the BR method drops very quickly and saturates in a white noise like behaviour for higher frequencies in region III. The reason for this is the big structures generating blade geometry and the RANS model working in the boundary layer of the blade while the AL does not have a geometry and it uses LES everywhere and therefore does not smooth out the wind field in the vicinity of the blade as has been discussed already for the sectional forces. It again has to be amplified that the BR case has the highest resolution in the blade region and therefore has the most reliable results. The difference between BEM and AL in the high frequency range in region III could be according to the missing damping, filtering and dynamic wake effects in the BEM case. The AL method uses a Gaussian filter to smooth out the forces along the blade and the wake is much more complex than in the static wake model of BEM. It has to be amplified, that especially for the torque, a transition from BEM to AL can not be made just by filtering the signals, because filtering corresponds to a drop in the PSD, which is not observed in the mid range.

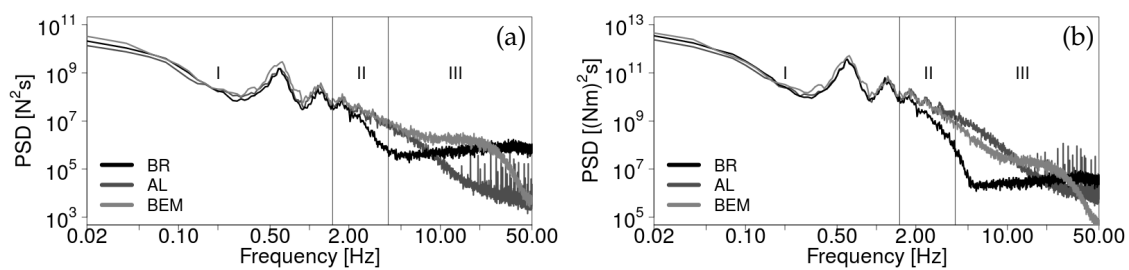


Figure 16. PSD of (a) thrust and (b) torque.

For a more detailed analysis, the cumulative frequency dependent variance normalized by the total variance, i.e.,

$$\hat{\sigma}^2(f) = \frac{\int_0^f PSD(f')df'}{\sigma^2} \tag{5}$$

has been investigated in Figure 17. This is equivalent to the energy content of the spectrum at frequencies smaller than f , normalized by the total energy contained in the spectrum. The energy content for the different regions can be determined as $\hat{\sigma}_{\text{region}}^2 = \hat{\sigma}^2(f_{\text{max}}) - \hat{\sigma}^2(f_{\text{min}})$ with f_{max} the upper frequency limit and f_{min} the lower frequency limit of the region. For all three methods the conclusion can be drawn that by far the most energy is contained in region I, in particular for the thrust: BR 95.4%, AL 93.3% and BEM 94.9%. Region II also contains a small amount of energy with 2.3% for BR, 5.8% for AL and 3.2% for BEM. The torque is distributed similarly with 97.7% for BR, 91.7% for AL and 91.1% for BEM in region I and 2.2%, 7.1% and 3.5% in region II. The variance contained in region III is negligible for both quantities. Based on the high percentage of variance contained in region I it can be concluded that the big difference in the total variance between BEM and the other two methods mainly stems from this frequency range. Therefore the extraction of wind fields at the position of the rotor plane has to be seen as a first step for this comparison and it has to be investigated if it is more appropriate to extract the fields downstream of the rotor position or to artificially damp the wind input in BEM on large scales.

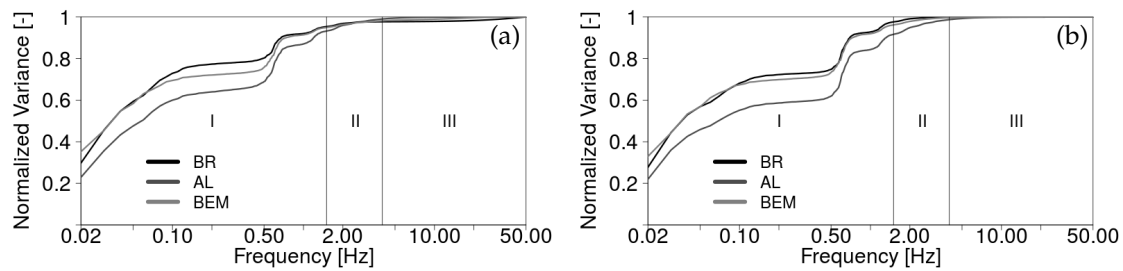


Figure 17. Normalized cumulative frequency dependent variance of (a) thrust and (b) torque.

4. Discussion

From this work it can be concluded that the AL, BR and the BEM method with extracted wind fields at the rotor plane from an empty domain are very similar with respect to averaged tangential and axial forces, except close to the root and the tip. However, a comparison of BEM with the CFD methods with respect to the standard deviations of sectional and integral forces shows very different results. For the integral quantities thrust and torque, BEM tends to overestimate the standard deviation compared to the other two methods. It was found out that the standard deviation differences between all methods mainly come from the different amplitudes in the first part of the spectrum and not from the filtering effects on larger frequencies. This leads to the conclusion that, if similar results for the standard deviation for BEM and CFD should be achieved, either the wind fields have to be extracted downwind of the rotor position from the empty domain simulation or a correction of wind fields for the BEM case has to be considered. A good starting point could be to substitute the equilibrium wake model by a dynamic wake model which could damp the oscillations and with it the standard deviation. This and extracting the wind fields in an empty domain downwind from the position where the turbine is normally located will be part of the future work. Another contribution to the differences, which also should not be neglected, comes from the fact that the turbulent wind field decays across the CFD domain due to the missing energy injection. In an empty domain, the turbulence intensity is higher upstream and lower downstream of the position, where the turbine would be located. This decay is not considered within the BEM simulation and could be a reason for the differences.

An indication for a linear dependence between standard deviation and EFL could be found for sectional as well as integral forces which seem to follow the same trend. This shows that the dynamics characterized by the EFL and by the standard deviation are similar for all three methods. However, this dependence is assumed to be existent only if the wind fields are comparable with respect to temporal and spatial correlations to assure similar turbulent structures which play a big role for EFL estimations. Out of scope of this paper, an advantage of this linear relationship could be that the computational expensive rainflow count algorithm is not needed if one is interested in equivalent fatigue loads. A simple calculation of the standard deviation could give this information as well. Additionally the equivalent fatigue loads could also be estimated if the same simulation is redone with a different standard deviation for the wind velocities.

Even if no experiments for comparison were performed, the BR simulation with its high resolution close to the blades and the full geometry consideration can be expected to be the most physical and therefore it should be seen as a benchmark case. However, a further part of the future work should be a fair comparison with experiments where the focus should be set on the statistical equivalence of the wind fields at least across the full rotor size in the CFD domain, in the BEM simulation and in the experiments.

Author Contributions: Conceptualization S.E., C.M.S. and H.R.; Software, S.E.; Methodology, S.E., C.M.S. and H.R.; Formal Analysis, S.E.; Writing-Original Draft Preparation, S.E. and H.R.; Writing-Review & Editing, J.P.; Supervision, J.P.; Project Administration, B.S.

Funding: This research received no external funding.

Acknowledgments: The simulations were performed at the HPC Cluster EDDY, located at the University of Oldenburg (Germany) and funded by the Federal Ministry for Economic Affairs and Energy (Bundesministerium für Wirtschaft und Energie) under grant number 0324005.

Conflicts of Interest: The authors declare no conflict of interest.

Abbreviations

The following abbreviations are used in this manuscript:

AL	Actuator Line
BEM	Blade Element Momentum
BR	Blade Resolved
CFD	Computational Fluid Dynamics
EFL	Equivalent Fatigue Loads
PSD	Power Spectral Density
TI	Turbulence Intensity

References

1. Schepers, J.G. Engineering Models in Wind Energy Aerodynamics. Ph.D. Thesis, Delft University of Technology, Delft, The Netherlands, 2012. [CrossRef]
2. International Electrotechnical Commission. *WIND TURBINES—PART 1: DESIGN REQUIREMENTS*; Standard IEC 61400-1; International Electrotechnical Commission: Geneva, Switzerland, 2005.
3. Madsen, H.A.; Sørensen, N.N.; Bak, C.; Troldborg, N.; Pirrung, G. Measured aerodynamic forces on a full scale 2MW turbine in comparison with EllipSys3D and HAWC2 simulations. *J. Phys. Conf. Ser.* **2018**, *1037*. [CrossRef]
4. Kim, Y.; Lutz, T.; Jost, E.; Gomez-Irardi, S.; Muñoz, A.; Méndez, B.; Lampropoulos, N.; Sørensen, N.; Madsen, H.; van der Laan, P.; et al. AVATAR Deliverable D2.5: Effects of Inflow Turbulence on Large Wind Turbines. AVATAR Deliverable D2.5, Technical Report. Available online: http://www.eera-avator.eu/fileadmin/avator/user/avator_D2p5_revised_20161231.pdf (accessed on 4 December 2018).
5. Mann, J. Wind field simulation. *Probabilistic Eng. Mech.* **1998**, *13*, 269–282. [CrossRef]
6. Sørensen, J.N.; Shen, W.Z. Numerical Modeling of Wind Turbine Wakes. *J. Fluids Eng.* **2002**, *124*, 393–399. [CrossRef]
7. Jonkmann, J.; Butterfield, S.; Musial, W.; Scott, G. *Definition of a 5-MW Reference Wind Turbine for Offshore System Development*; Technical Report TP-500-38060; National Renewable Energy Laboratory: Golden, CO, USA, 2009.
8. OpenCFD. *OpenFOAM—The Open Source CFD Toolbox—User’s Guide*; 1.4 ed.; OpenCFD Ltd.: Reading, UK, 2007.
9. Rahimi, H.; Daniele, E.; Stoevesandt, B.; Peinke, J. Development and application of a grid generation tool for aerodynamic simulations of wind turbines. *Wind Eng.* **2016**, *40*, 148–172. [CrossRef]
10. Rahimi, H. Validation and Improvement of Numerical Methods for Wind Turbine Aerodynamics. Ph.D. Thesis, University of Oldenburg: Oldenburg, Germany, 2018.
11. Rahimi, H.; Garcia, A.M.; Stoevesandt, B.; Peinke, J.; Schepers, J.G. An engineering model for wind turbines under yawed conditions derived from high fidelity models. *Wind Energy* **2018**, *21*, 618–633. [CrossRef]
12. Spalart, P.R.; Deck, S.; Shur, M.L.; Squires, K.D.; Strelets, M.K.; Travin, A. A New Version of Detached-eddy Simulation, Resistant to Ambiguous Grid Densities. *Theor. Comput. Fluid Dyn.* **2006**, *20*, 181. [CrossRef]
13. Patankar, S.; Spalding, D. A calculation procedure for heat, mass and momentum transfer in three-dimensional parabolic flows. *Int. J. Heat Mass Transfer* **1972**, *15*, 1787–1806. [CrossRef]
14. Issa, R. Solution of the implicitly discretised fluid flow equations by operator-splitting. *J. Comput. Phys.* **1986**, *62*, 40–65. [CrossRef]
15. Prandtl, L. *Ludwig Prandtl Gesammelte Abhandlungen: Zur Angewandten Mechanik, Hydro- und Aerodynamik*; Springer: Berlin, Germany, 2013.
16. Du, Z.; Selig, M. A 3-D stall-delay model for horizontal axis wind turbine performance prediction. In Proceedings of the 1998 ASME Wind Energy Symposium, Reno, NV, USA, 12–15 January 1998; p. 21.
17. Smagorinsky, J. General Circulation Experiments with the Primitive Equations. *Mon. Weather Rev.* **1963**, *91*, 99–164. [CrossRef]

18. Jonkman, B.; Jonkman, J. *FAST v8.16.00a-bjj*; Technical Report; NREL: Golden, CO, USA, 2016.
19. Jonkman, J.; Hayman, G.; Jonkman, B.; Damian, R. *AeroDyn v15 User's Guide and Theory Manual (Draft Version)*; Technical Report; NREL: Golden, CO, USA, 2016.
20. Leishman, J.G.; Beddoes, T.S. A Semi-Empirical Model for Dynamic Stall. *J. Am. Helicopter Soc.* **1989**, *34*, 3–17. [[CrossRef](#)]
21. Madsen, P.H. *Recommended Practices for Wind Turbine Testing and Evaluation. 3. Fatigue Loads*; Riso National Laboratory: Roskilde, Denmark, 1990.
22. Rychlik, I. A new definition of the rainflow cycle counting method. *Int. J. Fatigue* **1987**, *9*, 119–121. [[CrossRef](#)]
23. Martínez-Tossas, L.A.; Churchfield, M.J.; Leonardi, S. Large eddy simulations of the flow past wind turbines: Actuator line and disk modeling. *Wind Energy* **2015**, *18*, 1047–1060. [[CrossRef](#)]



© 2018 by the authors. Licensee MDPI, Basel, Switzerland. This article is an open access article distributed under the terms and conditions of the Creative Commons Attribution (CC BY) license (<http://creativecommons.org/licenses/by/4.0/>).